
Unsupervised Image-to-Image Translation Networks

Ming-Yu Liu, Thomas Breuel, Jan Kautz

NVIDIA, Santa Clara, California, USA

{MINGYUL,TBREUEL,JKAUTZ}@NVIDIA.COM

Abstract

Most of the existing image-to-image translation frameworks—mapping an image in one domain to a corresponding image in another—are based on supervised learning, i.e., pairs of corresponding images in two domains are required for learning the translation function. This largely limits their applications, because capturing corresponding images in two different domains is often a difficult task. To address the issue, we propose the UNsupervised Image-to-image Translation (UNIT) framework, which is based on variational autoencoders and generative adversarial networks. The proposed framework can learn the translation function without any corresponding images in two domains. We enable this learning capability by combining a weight-sharing constraint and an adversarial training objective. Through visualization results from various unsupervised image translation tasks, we verify the effectiveness of the proposed framework. An ablation study further reveals the critical design choices. Moreover, we apply the UNIT framework to the unsupervised domain adaptation task and achieve better results than competing algorithms do in benchmark datasets.

1. Introduction

Mapping images from one domain to another (image-to-image translation) has a wide range of applications. One may translate an image in a modality that is difficult to understand to a corresponding color image for better visualization; one may translate labeled images in one domain to corresponding images in a target domain, creating a training dataset that could be used for training classifiers in the target domain.

Most of the existing image-to-image translation approaches

are based on supervised learning. They require training datasets consisting of pairs of corresponding images in two domains (Ledig et al., 2016; Isola et al., 2016). Although they can achieve good performance in several image translation tasks (e.g. super-resolution and colorization), the required image pairs are difficult to obtain for many applications; certain applications require complex setups, involving multiple sensors, mirrors, and beam splitters, while other applications may require alterations to the appearances of human subjects.

To address this limitation, we propose using the UNsupervised Image-to-image Translation (UNIT) network framework to learn a two-way translation function between two image domains. Instead of requiring corresponding image pairs, we merely assume a dataset of images from each domain. The framework is based on recent deep generative models, including generative adversarial networks (GANs) and variational autoencoders (VAEs). We model each image domain using a VAE and a GAN. Through an adversarial training objective, an image fidelity function is implicitly defined for each domain. The adversarial training objective interacts with a weight-sharing constraint to generate corresponding images in two domains, while the variational autoencoders relate translated images with input images in the respective domains. Through visualization results from various unsupervised image translation tasks, we verify the effectiveness of the proposed framework. An ablation study and a hyperparameter sensitivity test reveal the critical design choices. Finally, we apply UNIT to the unsupervised domain adaptation task and achieve better results than competing algorithms do in the benchmark datasets.

2. Mathematical Motivation

Let \mathcal{X}_1 and \mathcal{X}_2 be two different image domains. In a supervised image-to-image translation problem, we are given training samples (x_1, x_2) drawn from a joint distribution $P_{\mathcal{X}_1, \mathcal{X}_2}(x_1, x_2)$. In the unsupervised setting, we are given training samples only from the marginal distributions $P_{\mathcal{X}_1}(x_1)$ and $P_{\mathcal{X}_2}(x_2)$. Without any other assumptions, we could infer nothing about the joint distribution from the marginal distributions.

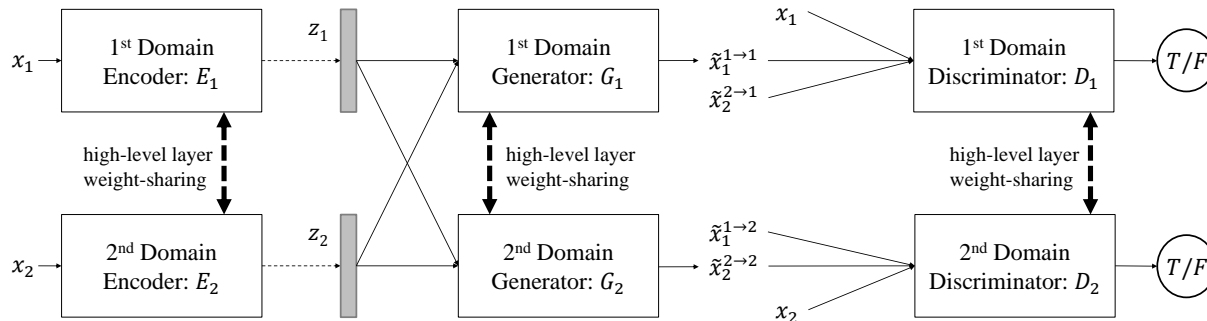


Figure 1: The UNsupervised Image-to-image Translation (UNIT) network has two encoders E_1 and E_2 , two generators G_1 and G_2 , and two adversarial discriminators D_1 and D_2 where E_1 , G_1 , and D_1 is for the first domain while E_2 , G_2 , and D_2 is for the second domain. They are all realized as convolutional neural networks. The encoder and generator pair in the same domain forms a variational autoencoder, while the generator and adversarial discriminator pair in the same domain forms a generative adversarial network. For an input image in the first domain x_1 , UNIT first encodes it using E_1 . The output latent code z_1 is then sampled and fed to both the first and second domain generators G_1 and G_2 to generate the reconstructed image $\hat{x}_1^{1 \rightarrow 1} = G_1(z_1 \sim q_1(z_1|x_1))$ and the domain translated image $\hat{x}_2^{1 \rightarrow 2} = G_2(z_1 \sim q_1(z_1|x_1))$, respectively. The two generated images are then judged by the adversarial discriminators D_1 and D_2 in the respective domains by their fidelity. Based on the intuition that a pair of corresponding images in different domains should share a same high-level image representation, we enforce several weight sharing constraints. The connection weights of the last few layers (high-level layers) in E_1 and E_2 are tied, the connection weights of the first few layers (high-level layers) in G_1 and G_2 are tied, and the connection weights of the last few layers (high-level layers) in D_1 and D_2 are tied. In the figure, a dotted line represents a sampling operation, while a solid line is a regular data flow. The bold dashed line represents the weight-sharing constraint.

In order to illustrate the motivation and idea behind our approach, let us consider a very simple model in which a nearly 1-1 correspondence between images in the two domains exists. (Of course, this is not generally true, such as the correspondence between thermal and RGB images, so we will talk about general cases in the next section.)

Recall that we are trying to discover the relationship between two related image domains \mathcal{X}_1 and \mathcal{X}_2 . Under the assumption of near perfect 1-1 correspondences between images in these two domains, given $x_1 \in \mathcal{X}_1$ and $x_2 \in \mathcal{X}_2$ a function $\phi^{1 \rightarrow 2}$ such that $x_2 \approx \phi^{1 \rightarrow 2}(x_1)$, and an inverse function $\phi^{2 \rightarrow 1}$ for the reverse mapping $x_1 = \phi^{2 \rightarrow 1}(x_2)$ exist. For the joint density, this means that $P_{\mathcal{X}_1, \mathcal{X}_2}(x_1, x_2) \approx P_{\mathcal{X}_1}(x_1)\delta(x_2 - \phi^{1 \rightarrow 2}(x_1))$, where δ is the Dirac delta function (this is reminiscent of the constraint used in (Viola & Wells III, 1997) for cross-domain image alignment). However, merely postulating a functional relationship (or even a smooth functional relationship) is not enough to infer a useful correspondence between \mathcal{X}_1 and \mathcal{X}_2 from samples drawn from the marginal distributions. We therefore require additional assumptions.

First, we assume that the relationship between \mathcal{X}_1 and \mathcal{X}_2 does not only exist at the image level but also at the level of local patches or regions. Similar to other deep networks, our model realizes this assumption through the use of convolutional layers. Then, we make an additional, strong assumption—for any given images x_1 and x_2 , there exists a common underlying representation z , such that we can recover both images from this underlying representation, and that we can compute this underlying representation from each of the two input images. That is, we postulate that

there exist functions E_1 , E_2 , G_1 and G_2 such that, given a sample (x_1, x_2) from the joint distribution, $z \approx E_1(x_1) \approx E_2(x_2)$ and conversely, $x_1 \approx G_1(z)$ and $x_2 \approx G_2(z)$. Within this model, the function $x_2 = \phi^{1 \rightarrow 2}(x_1)$ that maps from domain \mathcal{X}_1 to domain \mathcal{X}_2 can then be represented by the composition $\phi^{1 \rightarrow 2}(x_1) = E_2(G_1(x_1))$.

In more general image translation problems, the relationships between images and representations are only approximately functional. That is, a single thermal image may correspond to a whole range of color images, with uncertainty in both specific pixel color values (a kind of noise) and global color assignments. Therefore, instead of simply learning functional relations E_1 , E_2 , G_1 and G_2 between images and representations, we need to learn statistical distributions using a combination of VAEs and GANs. Furthermore, in the absence of supervised training data, we also need to devise an adversarial training procedure.

In the next section, we will discuss how we realize the above ideas using the UNIT framework.

3. The UNIT Framework

We propose the unsupervised image translation (UNIT) network framework for the unsupervised image-to-image translation task. The framework, as illustrated in Figure 1, is motivated by recent deep generative models including variational autoencoders (VAEs) (Kingma & Welling, 2013; Rezende et al., 2014; Larsen et al., 2016) and generative adversarial networks (GANs) (Goodfellow et al., 2014; Liu & Tuzel, 2016). It consists of 6 subnetworks: including two domain image encoders E_1 and E_2 , two domain

image generators G_1 and G_2 , and two domain adversarial discriminators D_1 and D_2 . Several ways exist to interpret the roles of the subnetworks as summarize in Table 1. We note that the UNIT network learns two-way translation in one shot. In the following, we first present the UNIT framework and then discuss the design considerations.

VAEs: The encoder-generator pair $\{E_1, G_1\}$ constitutes a VAE for the \mathcal{X}_1 domain, termed VAE₁. For an input image $x_1 \in \mathcal{X}_1$, the VAE₁ first maps it to a code in a latent space \mathcal{Z} via the encoder E_1 and then decodes a random-perturbed version of the code to reconstruct the input image via the generator G_1 . Following the VAE design in (Kingma & Welling, 2013) we assume the components in the latent space \mathcal{Z} are conditionally independent and Gaussian. The encoder outputs a mean vector $E_{1,\mu}(x_1)$ and a variance vector $E_{1,\sigma^2}(x_1)$ where the distribution of the latent code z_1 is given by $q_1(z_1|x_1) \equiv \mathcal{N}(z_1|E_{1,\mu}(x_1), \text{diag}(E_{1,\sigma^2}(x_1)))$. The diag operator converts a vector to a diagonal matrix where diagonal elements are the components of the vector. The reconstructed image is $\tilde{x}_1^{1 \rightarrow 1} = G_1(z_1 \sim q_1(z_1|x_1))$. Note that here we abused the notation where we treated the distribution of $q_1(z_1|x_1)$ as a random vector of $\mathcal{N}(E_{1,\mu}(x_1), \text{diag}(E_{1,\sigma^2}(x_1)))$ and sampled from it. This notation abuse avoided cluttered presentations, and several other instances of such a notation abuse can be found in the rest of the paper.

Similarly the pair of $\{E_2, G_2\}$ constitutes a VAE for the \mathcal{X}_2 domain: VAE₂. The encoder E_2 outputs a mean vector $E_{2,\mu}(x_2)$ and a variance vector $E_{2,\sigma^2}(x_2)$ and the distribution of the latent code z_2 is given by $q_2(z_2|x_2) \equiv \mathcal{N}(z_2|E_{2,\mu}(x_2), \text{diag}(E_{2,\sigma^2}(x_2)))$. The reconstructed image is denoted as $\tilde{x}_2^{2 \rightarrow 2} = G_2(z_2 \sim q_2(z_2|x_2))$.

Utilizing the reparameterization trick (Kingma & Welling, 2013), the non-differentiable sampling operation can be reparameterized as a differentiable arithmetic operation using auxiliary random variables. This reparameterization trick allows us to train the VAE using the standard backprop algorithm. Let η be a random vector with a multivariate Gaussian distribution: $\eta \sim \mathcal{N}(\eta|0, I)$. The sampling operation of $z_1 \sim q_1(z_1|x_1)$ can be implemented via $z_1 = E_{1,\mu}(x_1) + E_{1,\sigma^2}(x_1) \circ \eta$ where \circ is the Hadamard product. Similarly, the sampling operation of $z_2 \sim q_2(z_2|x_2)$ is implemented as $z_2 = E_{2,\mu}(x_2) + E_{2,\sigma^2}(x_2) \circ \eta$.

Weight-sharing: In order to relate the representations in the two VAEs, we enforce a weight-sharing constraint. We share the weights of the last few layers of E_1 and E_2 that are responsible for extracting high-level representations of the input images in the two domains based on the intuition that high-level representations of a pair of corresponding images in the two domains should be the same. Similarly, we share the weights of the first few layers of G_1 and G_2

Table 1: Interpretation of the roles of the subnetworks in UNIT.

Subnetworks	Role
$\{E_1, G_1\}$	VAE for \mathcal{X}_1
$\{E_2, G_2\}$	VAE for \mathcal{X}_2
$\{E_1, G_2\}$	$\mathcal{X}_1 \rightarrow \mathcal{X}_2$ Image Translator
$\{E_2, G_1\}$	$\mathcal{X}_2 \rightarrow \mathcal{X}_1$ Image Translator
$\{G_1, D_1\}$	GAN for \mathcal{X}_1
$\{G_2, D_2\}$	GAN for \mathcal{X}_2
$\{E_1, G_1, D_1\}$	VAE-GAN (Larsen et al., 2016)
$\{G_1, G_2, D_1, D_2\}$	CoGAN (Liu & Tuzel, 2016)

that are responsible for decoding high-level representations for reconstructing the input images¹.

Note that the weight-sharing constraint by itself makes no guarantee that a pair of corresponding images in the two domains will have the same latent code². The latent codes for a pair of corresponding images are different in general. Even if they were the same, the same latent component may have different semantic meanings in the two domains. Hence, the same latent code could still be decoded to output two unrelated images in the two domains. However, we will show that through adversarial training, a pair of corresponding images in the two domains will be mapped to a common latent code by E_1 and E_2 , respectively, and a latent code will be mapped to a pair of corresponding images in the two domains by G_1 and G_2 , respectively.

The shared latent space of \mathcal{X}_1 and \mathcal{X}_2 allows us to perform image-to-image translation. We can translate an image x_1 in \mathcal{X}_1 to an image in \mathcal{X}_2 through applying $G_2(z_1 \sim q_1(z_1|x_1))$. We term such an information processing stream as the image translation stream. Two image translation streams exist in the UNIT framework: $\mathcal{X}_1 \rightarrow \mathcal{X}_2$ and $\mathcal{X}_2 \rightarrow \mathcal{X}_1$. The two streams are trained jointly with the image reconstruction streams. Once we ensure that a pair of corresponding images are mapped to a same latent code and a same latent code is decoded to a pair of corresponding images, $(x_1, G_2(z_1 \sim q_1(z_1|x_1)))$ will form a pair of corresponding images. In other words, the composition of E_1 and G_2 functions is our $\phi^{1 \rightarrow 2}$ for unsupervised image-to-image translation discussed in Section 2, and the composition of E_2 and G_1 function is our $\phi^{2 \rightarrow 1}$.

GANs: A UNIT network employs two adversarial discriminators: D_1 and D_2 . For images sampled from the first domain dataset, D_1 should output true, while for images generated by G_1 , it should output false. The images generated by G_1 can be either a same domain reconstructed images $\tilde{x}_1^{1 \rightarrow 1} = G_1(z_1 \sim q_1(z_1|x_1))$ or a domain translated im-

¹Note that the relative positions, with respect to the input layers, of the high-level information processing layers in the encoder and decoder subnetworks are different. The former is in the back, while the latter is in the front.

²In the unsupervised setting, no pair of corresponding images in the two domains exists to train the network to output a same latent code for corresponding images.

age $\tilde{x}_2^{2 \rightarrow 1} = G_1(z_2 \sim q_2(z_2|x_2))$. Similarly, D_2 is trained to output true for images sampled from the second domain dataset and false for images generated from G_2 . We share the weights of the high-level layers of D_1 and D_2 based on the same intuition discussed above.

Learning: Training the UNIT network can be done through jointly solving the learning problems of the VAE₁, VAE₂, GAN₁ and GAN₂ for both the image reconstruction streams and the image translation streams:

$$\begin{aligned} \min_{E_1, G_1, E_2, G_2} \max_{D_1, D_2} & \mathcal{L}_{\text{VAE}_1}(E_1, G_1) + \mathcal{L}_{\text{VAE}_2}(E_2, G_2) \\ & + \mathcal{L}_{\text{GAN}_1}(E_1, G_1, D_1) + \mathcal{L}_{\text{GAN}_2}(E_2, G_2, D_2). \end{aligned} \quad (1)$$

Training a VAE is usually done via minimizing a variational upper bound of a negative log-likelihood function. In (1), the VAE object functions are given by

$$\begin{aligned} \mathcal{L}_{\text{VAE}_1}(E_1, G_1) &= \lambda_1 \mathbb{E}_{z_1 \sim q_1(z_1|x_1)} [-\log p_{G_1}(x_1|z_1)] \\ &+ \lambda_2 \text{KL}(q_1(z_1|x_1) || p_\eta(z_1)) \end{aligned} \quad (2)$$

$$\begin{aligned} \mathcal{L}_{\text{VAE}_2}(E_2, G_2) &= \lambda_1 \mathbb{E}_{z_2 \sim q_2(z_2|x_2)} [-\log p_{G_2}(x_1|z_1)] \\ &+ \lambda_2 \text{KL}(q_2(z_2|x_2) || p_\eta(z_2)) \end{aligned} \quad (3)$$

where the hyper-parameters λ_1 and λ_2 control the weights of the objective functions and KL stands for the Kullback-Leibler (KL) divergence. The KL divergence terms penalize deviation of the distribution of the latent code from the prior distribution. The regularization allows an easy way to sample from the latent space (Kingma & Welling, 2013). We model the conditional distribution p_{G_1} using a Gaussian given by $p_{G_1}(x_1|z_1) = \frac{1}{2} \exp(\frac{-\|x_1 - G_1(z_1)\|^2}{2})$. Hence, minimizing the negative log-likelihood term is equivalent to minimizing the Euclidean distance between the image and the reconstructed image. The same modeling is applied to p_{G_2} . The prior distribution is $p_\eta(z) = \mathcal{N}(z|0, I)$.

In (1), the GAN objective functions are given by

$$\begin{aligned} \mathcal{L}_{\text{GAN}_1}(E_1, G_1, D_1) &= \mathbb{E}_{x_1 \sim P_{\mathcal{X}_1}} [\log D_1(x_1)] \\ &+ \frac{1}{2} \mathbb{E}_{z_1 \sim q_1(z_1|x_1)} [\log(1 - D_1(G_1(z_1)))] \\ &+ \frac{1}{2} \mathbb{E}_{z_2 \sim q_2(z_2|x_2)} [\log(1 - D_1(G_1(z_2)))] \quad (4) \\ \mathcal{L}_{\text{GAN}_2}(E_2, G_2, D_2) &= \mathbb{E}_{x_2 \sim P_{\mathcal{X}_2}} [\log D_2(x_2)] \\ &+ \frac{1}{2} \mathbb{E}_{z_2 \sim q_2(z_2|x_2)} [\log(1 - D_2(G_2(z_2)))] \\ &+ \frac{1}{2} \mathbb{E}_{z_1 \sim q_1(z_1|x_1)} [\log(1 - D_2(G_2(z_1)))] \quad (5) \end{aligned}$$

The objective functions in (4) and (5) differ from the standard GAN objective function in that generated images come from two different distributions. For (4), the two distributions are $q_1(z_1|x_1)$ (the distribution of the reconstructed images for the input images in \mathcal{X}_1) and $q_2(z_2|x_2)$ (the distribution of the translated images for the input images in \mathcal{X}_2). Optimizing (4) encourages G_1 to output images sampled from both of the distributions resembling images from \mathcal{X}_1 . Similarly, optimizing (5) encourages G_2 to

output images sampled from $q_1(z_1|x_1)$ and $q_2(z_2|x_2)$ resembling images from \mathcal{X}_2 .

Inheriting from GAN, the UNIT training problem is a mini-max problem where the optimization is about finding a saddle point. It can be seen as a two player zero-sum game. The first player is a team consisting of the encoders and generators. The second player is a team consisting of the adversarial discriminators. In addition to defeating the second player, the first player has to minimize the VAE losses. We apply an alternating gradient update scheme similar to the one described in (Goodfellow et al., 2014) to solve (1). Specifically, we first apply a gradient ascent step to update D_1 and D_2 with E_1, E_2, G_1 , and G_2 fixed. We then apply a gradient descent step to update E_1, E_2, G_1 , and G_2 with D_1 and D_2 fixed. The details of the optimization algorithm are given in Algorithm 1 in the appendix.

Translation: Once the training is completed, we obtain two image translation functions by assembling a subset of the subnetworks in the UNIT network. We use the function $\phi^{1 \rightarrow 2}(x_1) = G_2(z_1 \sim q_1(z_1|x_1))$ for translating images from \mathcal{X}_1 to \mathcal{X}_2 , and use the function $\phi^{2 \rightarrow 1}(x_2) = G_1(z_2 \sim q_2(z_2|x_2))$ for translating images from \mathcal{X}_2 to \mathcal{X}_1 .

Discussion: We employ the VAEs in the UNIT framework for the following reasons: 1) VAEs are established generative models. 2) Sampling from the VAE latent space admits a simple form, allowing a seamless integration with GANs (Larsen et al., 2016). 3) Randomness injected in the VAE sampling step is useful for modeling the randomness in image translation: corresponding images with different appearances for the same input image can be generated with different realizations of the random perturbation³. Nevertheless, for the unsupervised image-to-image translation task, only using VAEs (instead of UNIT) would have the shortcoming that none of the terms in the objective function is defined on the translated images—no feedback is available to the image translation streams. Pure VAEs also tend to produce blurry images. In the UNIT framework, the GAN discriminators address these shortcomings. An image generator trained using the GAN loss can generate crisp sharp images (Larsen et al., 2016; Ledig et al., 2016). More importantly, the GAN discriminators are those that provide feedback to train the image translation streams.

Optimizing the GAN loss alone is insufficient for learning the image-to-image translation function in an unsupervised manner. The weight-sharing constraint is necessary for encouraging a generated image from an image translation stream resembles a translated version of the input image. The weight-sharing constraint sets an information

³The VAE implementation adopted in the paper is unimodal and cannot be used to model the multi-modal nature of image translation. We hypothesize a multi-modal VAE implementation would be necessary and leave it as the future work.

bottleneck. It limits the amount of representation power available at the high-level layers in the VAEs. If a VAE latent code represents two images of two different scenes in two different domains, then the two images will have to share the neurons at the high-level layers of the VAEs. Due to the sharing, each of the images will have difficulty to encode sufficient details to deceive the respective GAN discriminator. On the other hand, if the latent code represents two images of the same scene in two different domains, both of the images can utilize more capacity to deceive the discriminators, because many of the high-level concepts of the two images are the same. The information bottleneck gives incentives to generate corresponding images in two domains. Of course, when the capacity of the network is too large, there is no incentive for sharing the representation even with the weight-sharing constraint. In this case, the UNIT network fails to learn the translation function. We verify these points in the experiment section.

4. Implementations

Stochastic Skip Connections: The encoders in the UNIT network is responsible for mapping images to the latent space representing the image manifold. However, as the encoders get deeper, it becomes more difficult to preserve image details after layers of neural information processing. This results in blurry image reconstruction and translation. To overcome the issue, we apply skip connections to send intermediate image representations from the encoders to the decoders. The skip connections are applied to all the layers where the weights are shared by the two encoders. They create channels for transmitting image representations of different granularity. Note that we do not apply skip connections to the first few layers of the encoders where the weights are not shared because the representation computed by the layers are unavailable in the test time.

The skip connections in the UNIT network represent stochastic sampling operations, which complies with the VAE design principle. Let K be the number of skip connections. Note that the connection from the last encoder layer to the first decoder layer is considered as a skip connection for simplifying the discussion. The representations passed by the k th skip connection in E_1 and E_2 are random samples drawn from $z_{1,k} \sim q_{1,k}(z_{1,k}|x_1)$ and $z_{2,k} \sim q_{2,k}(z_{2,k}|x_2)$ where $q_{1,k}$ and $q_{2,k}$ are multi-variate Gaussian distributions whose means and covariance are given by the intermediate representations of the encoding layers that the skip connections are originated. The representations passed from the encoders to the decoders are hence concatenations of samples from the set of multi-variate Gaussian distributions: $z_1 \equiv (z_{1,1}, \dots, z_{1,K})$ and $z_2 \equiv (z_{2,1}, \dots, z_{2,K})$.

Spatial Context: We incorporate spatial-context informa-

tion for achieving a better image translation performance. For each input image, we create a y-image of the same size. The pixel values in the y-image are normalized y-coordinates where the bottom pixels have value 1 while the top pixels have value -1. The y-image is concatenated to the input image along the channel direction to create the final input image to the encoders as well as to the adversarial discriminators.

We trained the UNIT network using ADAM (Kingma & Ba, 2015). We set the learning rate to 0.0002 and momentums to 0.5 and 0.999, respectively, as in (Radford et al., 2016). The hyperparameters in the objective functions were set to $\lambda_1 = 0.0001$ and $\lambda_2 = 0.00001$ throughout the experiments. For translating large resolution images ($\geq 480 \times 480$), the batch size was set to 2 due to the limited memory size. Otherwise, the batch size was set to 64. We trained the UNIT networks using a Tesla P100 card in an NVIDIA DGX-1 machine. Training was typically done within a day. Our implementation will be made public.

5. Experiments

We first show the image translation results of the UNIT framework on several unsupervised image-to-image translation tasks. (More results are available in the appendix.) We then quantitatively analyze various design choices through an extensive set of experiments using a toy dataset. Finally, we apply the UNIT framework to the unsupervised domain adaptation task. Throughout the experiments, we emphasize no corresponding images exist in the training datasets for learning the translation function.

In the first experiment, we trained a UNIT network using the KAIST multispectral pedestrian detection benchmark (Hwang et al., 2015) for translating between day-time and night time images and between thermal IR and RGB images. The KAIST dataset contains several video sequences captured at different areas in a city at different times in a day. Some of the videos were captured at night time while the others were captured at day time. In addition to RGB video sequences, a thermal IR camera was used to capture thermal IR video sequences. The resolution of the RGB and thermal IR images in the videos were 640×512 . We operated in a transductive testing setting and translated the images in their original resolution. For the day-time and night-time image translation task, we created two datasets where the first set contained the images extracted from the day-time video sequences and the second set contained the images from the night-time sequences. The dataset sizes were 54,768 and 28,657 images, respectively. We applied the learned UNIT network to translate images in the two sets. The results are shown in Figure 2 and 3. We observed that UNIT translated day-time images to realistic and corresponding night-time images. The street lights were hal-

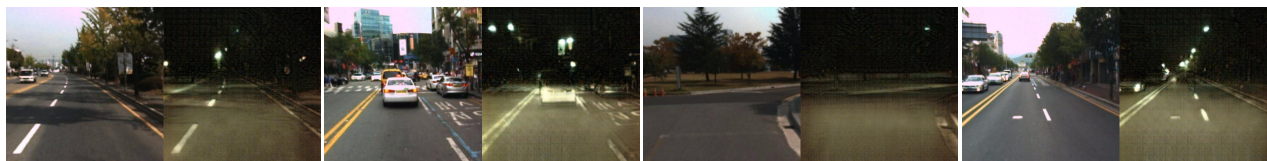


Figure 2: Results on Unsupervised Day-Image-to-Night-Image Translation. Left: input day image. Right: Output night image.

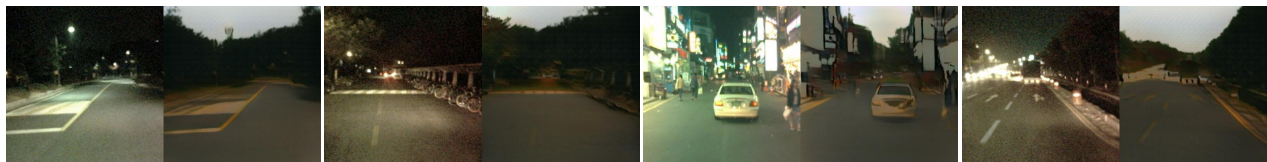


Figure 3: Results on Unsupervised Night-Image-to-Day-Image Translation. Left: input night image. Right: Output day image.



Figure 4: Results on Unsupervised Thermal-Image-to-RGB-Image Translation. Left: input thermal image. Right: Output color image.



Figure 5: Results on Unsupervised RGB-Image-to-Thermal-Image Translation. Left: input color image. Right: Output thermal image.



Figure 6: Results on Unsupervised Sunny-Image-to-Rainy-Image Translation. Left: input sunny image. Right: Output rainy image.

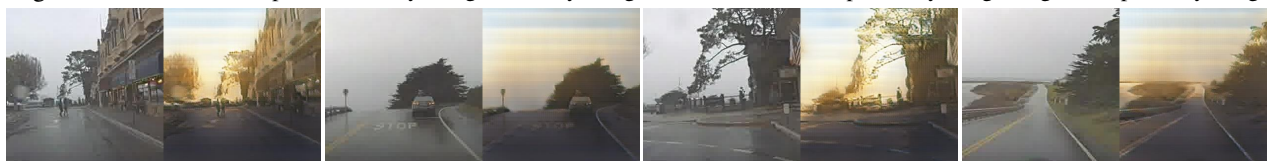


Figure 7: Results on Unsupervised Rainy-Image-to-Sunny-Image Translation. Left: input rainy image. Right: Output sunny image.

lucinated at plausible locations. The UNIT network also achieved good performance on night-time to day-time image translation.

We used the day-time video sequences in the KAIST dataset for training a UNIT for thermal IR and RGB image translation. We divided the sequences into two sets. For the first set, we only used the thermal IR images, while for the second set, we only used the RGB images. There were no corresponding thermal IR and RGB images in the two sets. The two sets contained 31,386 and 31,191 images, respectively. We applied the learned UNIT network to translate images in the two domains. The results are shown in Figure 4 and 5. We observed that the translation from thermal IR to RGB images were realistic. The color gradient in the tree region which were not observed in the thermal IR images were in the translated version. The translation from

RGB to thermal IR images were realistic too. The cloud texture patterns were removed in the generated thermal IR images, since the region has the same thermal signature.

We captured two datasets of driving sequences in California for training a UNIT for sunny and rainy image translation. The first set consisted of images captured on sunny days, while the second set consisted of images captured on rainy days. The datasets contained 11,863 and 2,267 images, respectively. We applied the learned UNIT network to translate images in the two domains. The results are shown in Figure 6 and 7. We found that clouds were added to the sky region and the images appear gloomy when translating from sunny to rainy. On the other hand, clouds were replaced with sunshine when translating images from rainy day to sunny day.

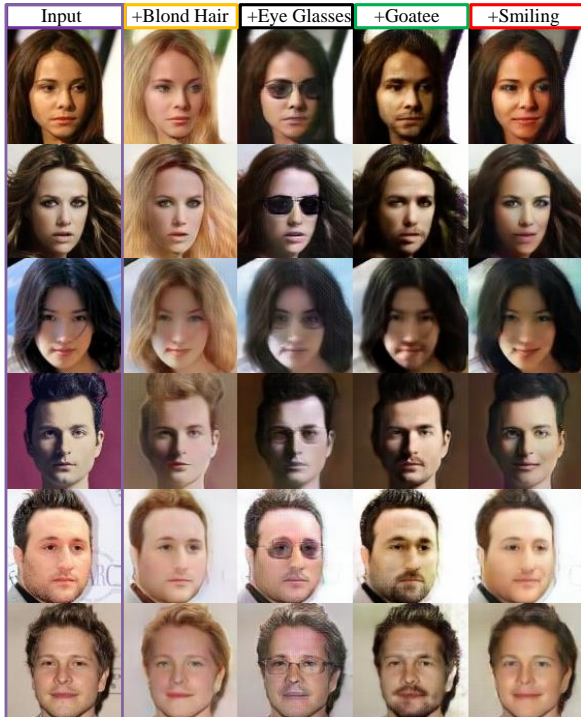


Figure 8: Attribute-based face image translation results.

We used the CelebFaces Attributes dataset (Liu et al., 2015) for translating face images based on attributes. Each face image in the dataset had several attributes, including blond hair, smiling, goatee, and eyeglasses. The face images with an attribute constituted the 1st domain, while those without the attribute constituted the 2nd domain. No corresponding face images between the two domains was given. We resized the images to a resolution of 132×132 and randomly sampled 128×128 regions for training. For each attribute translation, we trained a UNIT network. In Figure 8 we visualized the results where we translated several images that do not have blond hair, eye glasses, goatee, and smiling to corresponding images with each of the individual attributes. We found that the translated face images were realistic.

Quantitative Evaluation: Quantitative evaluation of generative models is known to be a challenging task and the popular metrics are all subject to flaws (Theis et al., 2016). Hence, we developed an evaluation protocol tailored for the unsupervised image translation task for studying impact of individual components in the UNIT framework. We used the MNIST dataset to create a toy dataset where the ground truth image translation function between two domains is known. Specifically we partitioned the MNIST training set into two equal-sized disjoint sets. For the digit images in the 1st set, we randomly colored the strokes in either red green or blue. For the images in the 2nd set, we first computed the edge images and then randomly colored the edges in either magenta yellow or cyan. We trained the UNIT network to learn the translation function between the two

digit domains. For our evaluation, we translated the images in the MNIST test set from one domain to the other and compared the Euclidean distance between an image that was translated by the learned UNIT translation function to the corresponding image that was translated by the ground truth translation function. Please find experimental details, performance numbers (average Euclidean distance of all the images in the MNIST test set) and an analysis on various design choices in the appendix. We briefly summarize our findings here:

- **Network Capacity:** When the capacity of a UNIT network was too low (e.g., a small number of neurons in each layer), the quality of the learned translation function degraded; however, when the capacity was too high, the UNIT network failed to learn the translation function at all. We concluded that setting a proper network capacity is very important for the UNIT framework.
- **Sensitivity to Hyperparameters:** We found that UNIT was not sensitive to the learning hyperparameters and a wide range of λ_1 and λ_2 values (see (2) and (3) for definitions) rendered comparable unsupervised image translation performance.
- **Weight-sharing:** We found that applying the weight-sharing constraint to the encoders and generators were essential. Without a sufficient number of weight-sharing layers, UNIT failed to learn the translation function.
- **Ablation Study:** We found that E_1 , E_2 , G_1 , G_2 , D_1 , and D_2 were all essential to the UNIT framework. When removing D_1 and D_2 , the resulting network became a coupled VAE network. It could still learn the translation function for the toy dataset but was inferior and outputted blurry images. When removing other subnetworks, the resulting network failed to learn the image translation function.

Unsupervised Domain Adaptation (UDA): We applied the UNIT framework to the UDA problem, i.e., adapting a classifier trained using labeled samples in one domain (source domain) to classify samples in a new domain (target domain) where labeled samples in the new domain are unavailable. A UDA algorithm has to leverage unlabeled samples in the new domain for adapting the classifier. Early UDA works have explored ideas from subspace learning (Fernando et al., 2013) to deep learning (Ganin et al., 2016; Liu & Tuzel, 2016; Taigman et al., 2017).

We used a multi-task learning approach where we trained a UNIT network to translate images between the source and target domains as well as trained the adversarial discriminator in the source domain to classify samples in the source domain. Due to the weight-sharing constraint enforced in the high-level layers in the adversarial discriminators, the trained adversarial discriminator in the target domain can classify samples in the target domain, inheriting the

Table 2: UDA results on adapting from the SVHN domain to the MNIST domain. The results of the other algorithms were duplicated from (Taigman et al., 2017)

Method	Accuracy
SA (Fernando et al., 2013)	59.32%
DANN (Ganin et al., 2016)	73.85%
DTN (Taigman et al., 2017)	84.88%
UNIT (proposed)	90.53%

power from the source domain discriminator. We did not use a separately trained source-domain classifier to classify UNIT-translated samples because the multi-task learning approach performed better in practice, possibly due to the use of unlabeled data in the target domain in training.

We applied the above approach to the task of adapting a classifier from the Street View House Number (SVHN) dataset (Netzer et al., 2011) to the MNIST dataset. Specifically, we trained the UNIT network to learn to translate images between the SVHN and MNIST training sets as well as to classify the digit classes in the SVHN training images using the features extracted by the SVHN domain adversarial discriminators. During test time, we applied the target domain adversarial discriminator to classify the digit class in the MNIST test set. We reported the achieved performance with comparison to the competing methods in Table 9. We found that our approach achieved a 90.53% accuracy, which was much better than 84.88% achieved by the previous state-of-the-art method (Taigman et al., 2017). The details of the network architecture and additional experiments are available in the supplementary materials.

6. Related Works

Several deep generative models were recently proposed for image generation including GANs (Goodfellow et al., 2014), VAEs (Kingma & Welling, 2013; Rezende et al., 2014), moment matching networks (Li et al., 2015), PixelCNN (van den Oord et al., 2016), and Plug&Play Generative Networks (Nguyen et al., 2016). The UNIT framework was based on GANs and VAEs but it was designed for the unsupervised image-to-image translation task. In the following, we first review several recent GAN and VAE works and then discuss related image translation works.

GANs learn to generate images by setting up a zero-sum game played by a generator and a discriminator. The quality of images generated by GANs had improved dramatically since its introduction. (Denton et al., 2015) proposed a Laplacian pyramid implementation of GANs. (Radford et al., 2016) used a deeper convolution network architecture. (Zhang et al., 2016) stacks two generators to progressively render realistic images. InfoGAN (Chen et al., 2016) learned to a more interpretable latent representation. (Salimans et al., 2016) proposed several GAN training tricks. (Arjovsky et al., 2017) proposed the Wasserstein

GAN framework for a more stable GAN training.

VAEs optimize a variational bound of the image likelihood function. By improving the variational approximation, better image generation results were achieved (Maaløe et al., 2016; Kingma et al., 2016). In (Larsen et al., 2016), a VAE-GAN architecture was proposed to improve image generation quality of VAEs. VAEs were applied to translate face image attribute in (Yan et al., 2016).

Image Translation via a conditional generative model is now a popular approach for mapping an image from one domain to the other. Most of the existing works were based on supervised learning (Ledig et al., 2016; Isola et al., 2016), requiring corresponding images in two domains. Our work differed to the previous works in that we do not need corresponding images. Recently, (Taigman et al., 2017) proposed the domain transformation network (DTN) and achieved promising results on translating small resolution face and digit images. In addition to faces and digits, the UNIT network can translate large resolution natural images. It also achieved a better performance in the unsupervised domain adaptation task. In (Shrivastava et al., 2016), a conditional generative adversarial network-based approach was proposed to translate a rendering images to a real image for gaze estimation. In order to ensure the generated real image was similar to the original rendering image, the L1 distance between the generated and original image was minimized. While this approach could generate more realistic rendering images, it is not applicable to the natural image translation task. For example, for the task of converting a thermal image to a color image, the L1 distance between a translated color image and the input thermal image does not carry meaningful senses.

We note that image translation is different to style transfer (Gatys et al., 2016; Johnson et al., 2016) in that while style transfer focuses on translate a natural image to an abstract, artistic image, image translation also considers translating a natural image to another natural image where loss of image details is unacceptable.

7. Conclusion and Future Work

We presented the UNIT framework—a general framework for unsupervised image-to-image translation. We showed it learned to translate an image from one domain to another without any corresponding images in two domains in the training dataset. In future, we plan to extend the framework to deal with the semi-supervised image-to-image translation task where supervision of domain correspondence is given either through a set of rules or a few pairs of corresponding images. We are also interested in extending the framework to the unsupervised language-to-language translation task.

References

- Arjovsky, Martin, Chintala, Soumith, and Bottou, Léon. Wasserstein gan. *arXiv preprint arXiv:1701.07875*, 2017.
- Chen, Xi, Duan, Yan, Houthoofd, Rein, Schulman, John, Sutskever, Ilya, and Abbeel, Pieter. Infogan: Interpretable representation learning by information maximizing generative adversarial nets. In *Advances in Neural Information Processing Systems*, 2016.
- Denton, Emily L, Chintala, Soumith, Fergus, Rob, et al. Deep generative image models using a laplacian pyramid of adversarial networks. In *Advances in Neural Information Processing Systems*, 2015.
- Fernando, Basura, Habrard, Amaury, Sebban, Marc, and Tuytelaars, Tinne. Unsupervised visual domain adaptation using subspace alignment. In *International Conference on Computer Vision*, 2013.
- Ganin, Yaroslav, Ustinova, Evgeniya, Ajakan, Hana, Germain, Pascal, Larochelle, Hugo, Laviolette, François, Marchand, Mario, and Lempitsky, Victor. Domain-adversarial training of neural networks. *Journal of Machine Learning Research*, 2016.
- Gatys, Leon A, Ecker, Alexander S, and Bethge, Matthias. Image style transfer using convolutional neural networks. In *Conference on Computer Vision and Pattern Recognition (CVPR)*, 2016.
- Goodfellow, Ian, Pouget-Abadie, Jean, Mirza, Mehdi, Xu, Bing, Warde-Farley, David, Ozair, Sherjil, Courville, Aaron, and Bengio, Yoshua. Generative adversarial nets. In *Advances in Neural Information Processing Systems*, 2014.
- Hwang, Soonmin, Park, Jaesik, Kim, Namil, Choi, Yukyung, and So Kweon, In. Multispectral pedestrian detection: Benchmark dataset and baseline. In *Conference on Computer Vision and Pattern Recognition (CVPR)*, 2015.
- Isola, Phillip, Zhu, Jun-Yan, Zhou, Tinghui, and Efros, Alexei A. Image-to-image translation with conditional adversarial networks. *arXiv preprint arXiv:1611.07004*, 2016.
- Johnson, Justin, Alahi, Alexandre, and Fei-Fei, Li. Perceptual losses for real-time style transfer and super-resolution. In *European Conference in Computer Vision*, 2016.
- Kingma, Diederik and Ba, Jimmy. Adam: A method for stochastic optimization. In *International Conference on Learning Representations*, 2015.
- Kingma, Diederik P and Welling, Max. Auto-encoding variational bayes. *arXiv preprint arXiv:1312.6114*, 2013.
- Kingma, Diederik P, Salimans, Tim, and Welling, Max. Improving variational inference with inverse autoregressive flow. *arXiv preprint arXiv:1606.04934*, 2016.
- Larsen, Anders Boesen Lindbo, Sønderby, Søren Kaae, Larochelle, Hugo, and Winther, Ole. Autoencoding beyond pixels using a learned similarity metric. *International Conference on Machine Learning*, 2016.
- Ledig, Christian, Theis, Lucas, Huszár, Ferenc, Caballero, Jose, Cunningham, Andrew, Acosta, Alejandro, Aitken, Andrew, Tejani, Alykhan, Totz, Johannes, Wang, Zehan, et al. Photo-realistic single image super-resolution using a generative adversarial network. *arXiv preprint arXiv:1609.04802*, 2016.
- Li, Yujia, Swersky, Kevin, and Zemel, Richard S. Generative moment matching networks. In *International Conference on Machine Learning*, 2015.
- Liu, Ming-Yu and Tuzel, Oncel. Coupled generative adversarial networks. In *Advances in Neural Information Processing Systems*, 2016.
- Liu, Ziwei, Luo, Ping, Wang, Xiaogang, and Tang, Xiaoou. Deep learning face attributes in the wild. In *International Conference on Computer Vision*, 2015.
- Maaløe, Lars, Sønderby, Casper Kaae, Sønderby, Søren Kaae, and Winther, Ole. Auxiliary deep generative models. *arXiv preprint arXiv:1602.05473*, 2016.
- Netzer, Yuval, Wang, Tao, Coates, Adam, Bissacco, Alessandro, Wu, Bo, and Ng, Andrew Y. Reading digits in natural images with unsupervised feature learning. In *Advances in Neural Information Processing Systems workshop*, 2011.
- Nguyen, Anh, Yosinski, Jason, Bengio, Yoshua, Dosovitskiy, Alexey, and Clune, Jeff. Plug & play generative networks: Conditional iterative generation of images in latent space. *arXiv preprint arXiv:1612.00005*, 2016.
- Radford, Alec, Metz, Luke, and Chintala, Soumith. Unsupervised representation learning with deep convolutional generative adversarial networks. In *International Conference on Learning Representations*, 2016.
- Rezende, Danilo Jimenez, Mohamed, Shakir, and Wierstra, Daan. Stochastic backpropagation and variational inference in deep latent gaussian models. In *International Conference on Machine Learning*, 2014.

- Salimans, Tim, Goodfellow, Ian, Zaremba, Wojciech, Cheung, Vicki, Radford, Alec, and Chen, Xi. Improved techniques for training gans. In *Advances in Neural Information Processing Systems*, 2016.
- Shrivastava, Ashish, Pfister, Tomas, Tuzel, Oncel, Susskind, Josh, Wang, Wenda, and Webb, Russ. Learning from simulated and unsupervised images through adversarial training. *arXiv preprint arXiv:1612.07828*, 2016.
- Taigman, Yaniv, Polyak, Adam, and Wolf, Lior. Unsupervised cross-domain image generation. *International Conference on Learning Representations*, 2017.
- Theis, Lucas, Oord, Aäron van den, and Bethge, Matthias. A note on the evaluation of generative models. *International Conference on Learning Representations*, 2016.
- van den Oord, Aaron, Kalchbrenner, Nal, Espeholt, Lasse, Vinyals, Oriol, Graves, Alex, et al. Conditional image generation with pixelcnn decoders. In *Advances in Neural Information Processing Systems*, 2016.
- Viola, Paul and Wells III, William M. Alignment by maximization of mutual information. *International journal of computer vision*, 24(2):137–154, 1997.
- Yan, Xinchun, Yang, Jimei, Sohn, Kihyuk, and Lee, Honglak. Attribute2image: Conditional image generation from visual attributes. *European Conference in Computer Vision*, 2016.
- Zhang, Han, Xu, Tao, Li, Hongsheng, Zhang, Shaoting, Huang, Xiaolei, Wang, Xiaogang, and Metaxas, Dimitris. Stackgan: Text to photo-realistic image synthesis with stacked generative adversarial networks. *arXiv preprint arXiv:1612.03242*, 2016.

A. Training

We present the learning algorithm for the UNIT framework in Algorithm 1. The algorithm can be considered as an extension of the learning algorithm for the generative adversarial networks (GAN). The convergence property follows the results shown in (Goodfellow et al., 2014).

Algorithm 1 The alternating stochastic gradient update algorithm for training the unsupervised image-to-image translation networks.

- 1: Initialize E_1 E_2 G_1 G_2 D_1 and D_2 with the shared network connection weights set to the same values.
- 2: **for** $t = 0, 1, 2, \dots, \text{MAX ITER}$ **do**
- 3: **for** $k = 0, 1, 2, \dots, K$ **do**
- 4: Draw N samples from the first domain training dataset, $X_1 = \{x_1^{(1)}, \dots, x_1^{(N)}\}$
- 5: Draw N samples from the second domain training dataset, $X_2 = \{x_2^{(1)}, \dots, x_2^{(N)}\}$
- 6: Draw N samples from p_η , $Z = \{z^{(1)}, \dots, z^{(N)}\}$
- 7: Perform a forward pass of the network using X_1 , X_2 , and Z .
- 8: Perform a backward pass of the network by backprop the gradients from the derivatives of

$$\mathcal{L}_{\text{GAN}_1}(E_1, G_1, D_1) + \mathcal{L}_{\text{GAN}_2}(E_1, G_2, D_2) \quad (6)$$

- 9: Update D_1 and D_2 using the gradients.
- 10: **end for**
- 11: Draw N samples from the first domain training dataset, $X_1 = \{x_1^{(1)}, \dots, x_1^{(N)}\}$
- 12: Draw N samples from the second domain training dataset, $X_2 = \{x_2^{(1)}, \dots, x_2^{(N)}\}$
- 13: Draw N samples from p_η , $Z = \{z^{(1)}, \dots, z^{(N)}\}$
- 14: Perform a forward pass of the network using X_1 , X_2 , and Z .
- 15: Perform a backward pass of the network by backprop the gradients from the derivatives of

$$\mathcal{L}_{\text{VAE}_1}(E_1, G_1) + \mathcal{L}_{\text{VAE}_2}(E_1, G_2) + \mathcal{L}_{\text{GAN}_1}(E_1, G_1, D_1) + \mathcal{L}_{\text{GAN}_2}(E_1, G_2, D_2) \quad (7)$$

- 16: Update E_1 E_2 G_1 and G_2 using the gradients.
- 17: **end for**

B. Quantitative Analysis

We created a toy dataset using the MNIST dataset for analyzing various components in the UNIT framework. We partitioned the MNIST training set into two equal-size disjoint sets. For each handwritten digit image in the first set, we randomly colored the strokes with a color that is either red, green, or blue. For each image in the second set, we first computed the edge map and then randomly colored the



Figure 9: Illustration of the toy dataset. Images in the left-hand side are from the first domain, while those in the right-hand side are from the second domain.

Table 3: The UNIT network architecture for the quantitative analysis. N=Neurons, K=Kernel size, S=Stride size, BN=Batch Normalization

Layer	Encoders	Shared?
1	CONV-(N32,K5,S2), BN, LeakyReLU	No
2	CONV-(N64,K5,S2), BN, LeakyReLU	Yes
3	CONV-(N128,K8,S1), BN, LeakyReLU	Yes
4	CONV-(N256,K1,S1), BN, LeakyReLU	Yes
μ	CONV-(N256,K1,S1)	Yes
σ^2	CONV-(N256,K1,S1), Soft-plus	Yes
Layer	Generators	Shared?
1	DCONV-(N256,K4,S2), BN, LeakyReLU	Yes
2	DCONV-(N128,K4,S2), BN, LeakyReLU	Yes
3	DCONV-(N64,K4,S2), BN, LeakyReLU	Yes
4	DCONV-(N32,K4,S2), BN, LeakyReLU	No
5	DCONV-(N3,K1,S1), TanH	No
Layer	Discriminators	Shared?
1	CONV-(N32,K5,S2), BN, LeakyReLU	No
2	CONV-(N64,K5,S2), BN, LeakyReLU	Yes
3	CONV-(N128,K8,S1), BN, LeakyReLU	Yes
4	CONV-(N256,K1,S1), BN, LeakyReLU	Yes
5	CONV-(N1,K2,S1), Sigmoid	Yes

edges with a color that is either cyan, yellow, or magenta. Some examples images from the two sets are illustrated in Figure 9.

The two sets formed two different image domains. Our goal was to translate a digit image from the 1st domain to the corresponding digit image in the 2nd domain and vice versa. Since no corresponding images existed in the two sets, the translation function learning had to be performed in an unsupervised manner. For performance evaluation, we translated the images in the MNIST *test set* from one domain to the other. For this toy dataset, we knew precisely what the translation function between the two domains was, which allowed us to quantitatively evaluate the performance of a learned translation function⁴. We computed the Euclidean distance between an image that was translated with the learned UNIT translation function to an image that was translated with the ground truth translation

⁴Note that we ignored the color difference as evaluating the translation performance. A digit in red color can perfectly match an edge image of the digit in either cyan, yellow, or magenta as long as the colored portion of the edge image resembles the edges extracted from the colored portion of the digit image.

function. The smaller the Euclidean distance between the two images, the closer the learned translation function to the ground truth translation function. We used the average Euclidean distance between the UNIT translated images and the ground-truth translated images in the test set as the performance metric for performance evaluation.

Sensitivity to Hyperparameters: The weights on the image likelihood terms, λ_1 , and the KL divergence terms, λ_2 , are two learning hyperparameters in the UNIT framework. To study their impact on the translation performance, we trained a UNIT network with different hyperparameter values. The encoders, generators, and discriminators used in the experiments were all five-layer convolutional networks. We applied weight-sharing to the last four layers of the encoders, the first three layers of the generators, and the last four layers of the discriminators. The UNIT network had 32 convolutional filters in the first layer and the number of filters for every next layer was doubled. For the toy dataset, we did not find a need to use skip connections. The details of the UNIT network is shown in Table 3.

In Figure 10 we fixed $\lambda_2 = 0.0001$ and plotted the translation error as a function of training iterations with different λ_1 values. The λ_1 values tested ranged from 0.001 to 100. The UNIT framework learned two-way translation simultaneously. We plotted the error curves for both translation directions. From the figure, we found that the performance of the translation functions did not depend on the hyperparameter values much for the toy dataset. A wide range of parameter values rendered good translation performance. However, we suspected that a hyperparameter search for the weight on the image likelihood term would still be necessary when dealing with natural image translation tasks. In Figure 11, we fixed $\lambda_1 = 1$ and plotted the translation errors as a function of training iterations with different λ_2 values. The λ_2 values tested ranged from 0.00001 to 0.1. Similar to the λ_1 case, we found that the performance of the translation functions did not depend on the hyperparameter values much. We set $\lambda_1 = 1$ and $\lambda_2 = 0.0001$ for the rest of the experiments in the section. Several digit translation results from this set of hyperparameters are visualized in Figure 13.

Network Capacity: The weight-sharing constraint in the UNIT framework limits the capacity of the encoders and generators, which enables UNIT to unsupervisedly learn the target image-to-image translation function. To understand the relation between the capacity and the quality of the learned translation function, we trained a set of UNIT networks with different numbers of convolutional filters. We kept the architecture of the discriminators fixed as in Table 3 (i.e. starting with 32 filters) and varied the number of filters in the encoders and generators. We tested five different versions of the UNIT networks. They started with

8, 16, 32, 64, and 128 filters in the first encoder layers, respectively. We doubled the number of filters for every next layer in the encoders. The number of convolutional filters in the first layers of the generators was set to equal to the number of convolutional filters in the last layers of the encoders. We halved the number of filters for every next layer in the generators. The UNIT network that had more filters in a convolutional layer had a higher capacity. We quantitatively evaluated the performance of the learned translation functions of the UNIT networks. The results are shown in Figure 12. From the figure, we observed that when the capacity was too low, the learned translation function did not perform well. But when the capacity was too high, the UNIT network failed to learn the translation function completely. As visualizing the translated images by the UNIT networks with high capacity, we found that the translated images were simply duplications of the input images. Figure 12 also showed that the network that starting with 32 convolutional filters rendered the best performance. However, we expected that the optimal number of filters would vary for different image translation tasks.

Weight-sharing: We conducted the following experiment to understand the role of weight-sharing in the UNIT framework. We trained a set of UNIT networks with different number of weight-sharing layers in the encoders, generators, and discriminators. The networks used in the experiment were all based on the architecture in Table 3. We trained the networks for 10K iterations and reported the performance in Table 4. We observed that the translation performance was invariant to the number of weight-sharing layers in the adversarial discriminators. In contrast, the performance largely depended on the number of weight-sharing layers in the encoders and decoders. Generally, with more weight-sharing layers, UNIT learned a better translation function. When the number of weight-sharing layers was too small, UNIT failed to learn the translation function completely.

Ablation Study: We conducted an ablation study to understand the dependency on each of the subnetworks in the UNIT framework. We trained several variants of the UNIT networks with various individual subnetworks removed. The architecture of the networks were all based on Table 3. In one experiment, we removed both of the adversarial discriminators. This rendered a pair of VAEs with a weight sharing constraint, which we refer to as the coupled VAEs. In another experiment, we removed the encoder in the second image domain. We have also tested removing the generator and adversarial discriminator in the second domain. This broke the symmetry in the UNIT framework and forced the remaining components in the UNIT network to focus on translating images from the second domain to the first domain. We trained these variants using the same hyperparameters and reported the performance in Table 5.

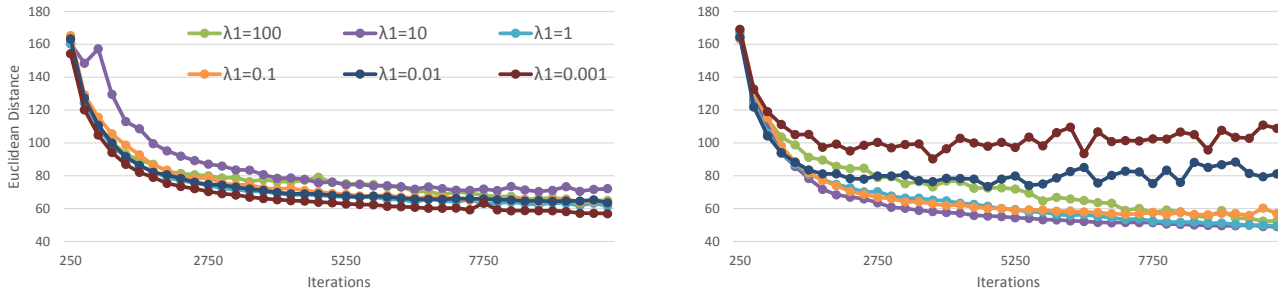


Figure 10: Sensitivity to the weight on the image likelihood term. The figure plots the translation error as a function of the training iteration with $\lambda_2 = 0.0001$ and λ_1 varying from 0.001 to 10000. Left: translation errors from the 1st domain to the 2nd domain. Right: translation errors from the 2nd domain to the 1st domain

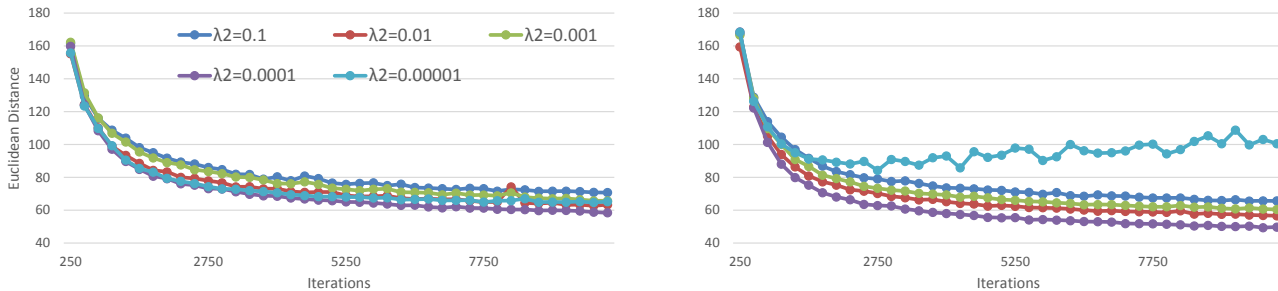


Figure 11: Sensitivity to the weight on the KL divergence term. The figure plots the translation error as a function of the training iteration with $\lambda_1 = 1.0$ and λ_2 varying from 0.000001 to 0.1. Left: translation errors from the 1st domain to the 2nd domain. Right: translation errors from the 2nd domain to the 1st domain

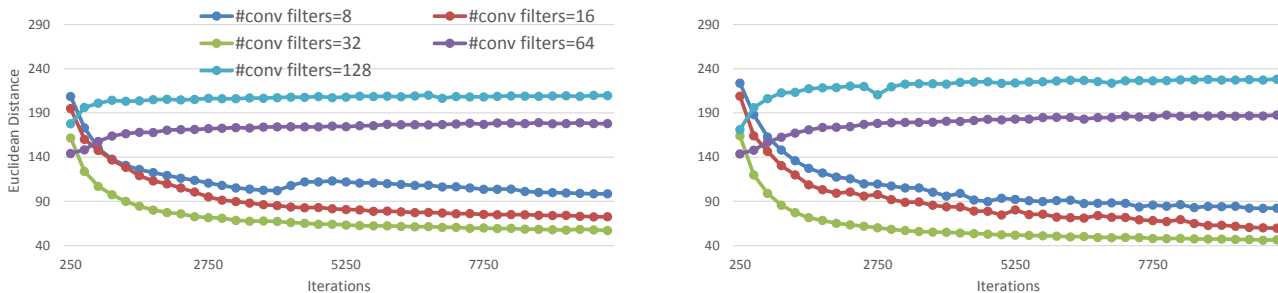


Figure 12: Network capacity versus translation performance. The figure plots the translation error as a function of the training iterations with a set of UNIT networks with different capacity values. Left: translation errors from the 1st domain to the 2nd domain. Right: translation errors from the 2nd domain to the 1st domain

From the table, we found that the UNIT network achieved the best translation performance, while the coupled VAEs was ranked second. Although the coupled VAEs rendered a comparable performance for the toy dataset, it produced blurred images as applied to natural images. We hence do not recommend it for the image translation task. From the table, we also found that the versions of the networks that broke the symmetry in the architecture failed to learn the translation function. We hypothesized that the failure was due to the absent of the weight-sharing constraint.

C. Unsupervised Domain Adaptation

We applied the UNIT framework to the UDA problem, which concerns adapting a classifier trained using labeled

samples in one domain, which is referred to as the source domain, to classify samples in a new domain, which is referred to as the target domain, where labeled samples in the new domain are unavailable. A UDA algorithm has to leverage unlabeled samples in the new domain for adapting the classifier.

We developed a multi-task learning approach where we trained a UNIT network to translate images between the source and target domains as well as trained the adversarial discriminator in the source domain in the UNIT network to classify samples in the source domain. Due to the weight-sharing constraint enforced in the high-level layers in the adversarial discriminators, the trained adversarial discriminator in the target domain in the UNIT network can classify samples in the target domain, inheriting the classification

Table 4: Number of weight-sharing layers versus translation performance. The numbers shown in the table are the average Euclidean distance between images translated by the learned UNIT translation function (after 10K iterations of training) and images translated by the ground truth translation function. The smaller the number the better the translation performance. In the x -axis, we vary n_E , which denotes the number of weight-sharing layers in E_1 and E_2 . In the y -axis, we vary n_G and n_D , which are the number of weight-sharing layers in G_1 and G_2 and the number of weight-sharing layers in D_1 and D_2 , respectively.

Translation from		n_D				
\mathcal{X}_1 to \mathcal{X}_2		4	3	2	1	0
(n_E, n_G)	(4, 3)	59.3	58.4	58.6	65.1	57.3
	(3, 2)	67.7	73.0	63.7	64.4	75.9
	(2, 1)	126.7	97.6	139.7	138.3	124.5
	(1, 0)	180.6	180.9	179.3	182.3	180.1
	(0, 0)	186.2	188.8	182.8	183.7	185.6

Translation from		n_D				
\mathcal{X}_2 to \mathcal{X}_1		4	3	2	1	0
(n_E, n_G)	(4, 3)	47.0	49.6	49.2	60.6	46.7
	(3, 2)	59.8	66.7	56.1	55.7	69.1
	(2, 1)	117.2	86.2	130.4	129.6	113.7
	(1, 0)	185.9	185.9	184.4	185.6	184.1
	(0, 0)	197.0	197.2	195.3	193.7	194.5



Figure 13: Visualization of the digit translation results. Left: Translation from the first domain to the second domain. Right: Translation from the second domain to the first domain. For each image pair, the one in the left-hand side is the input image, while the one in the right-hand side is the translated image.

power from the source domain adversarial discriminator. We did not use a separately trained source-domain classifier to classify UNIT-translated samples because the multi-task learning approach performed better in practice, possibly due to the use of unlabeled data in the target domain in training.

In the first UDA experiment, we applied the above approach to the task of adapting a classifier between the MNIST dataset and the USPS dataset. For the USPS dataset, we randomly partitioned it into two sets. One for training and the other for testing. The size of the training set was 4 times larger than the test set. We used a UNIT network where the encoder and decoder architecture were the same as those shown in Table 3. But the adversarial discriminators were based on the LeNet architecture as shown in Table 6. The adversarial discriminators had two different output layers: the first output layer has a single output neuron representing the probability that an input sample was from the training dataset (4a in Table 6) and the other out-

Table 5: Ablation Study. The numbers in the table are the average Euclidean distance between images translated by the learned translation function (after 10K iterations of training) and images translated by the ground truth translation function. The smaller the number the better the translation performance.

Subnetworks included	$\mathcal{X}_1 \rightarrow \mathcal{X}_2$	$\mathcal{X}_2 \rightarrow \mathcal{X}_1$
$E_1, E_2, G_1, G_2, D_1, D_2$ (UNIT)	59.3	47.0
E_1, E_2, G_1, G_2 (Coupled VAEs)	66.3	59.0
E_1, G_1, G_2, D_1, D_2	292.0	N/A
E_2, G_1, G_2, D_1, D_2	N/A	297.8
E_1, E_2, G_1, D_1	N/A	186.6
E_1, E_2, G_2, D_2	176.5	N/A

Table 6: The adversarial discriminator architecture for the MNIST-USPS domain adaptation problem.

Layer	Discriminators	Shared?
1	CONV-(N20,K5,S1), MaxPooling-(K2,S2)	No
2	CONV-(N50,K5,S1), MaxPooling-(K2,S2)	Yes
3	FC-(N500), ReLU, Dropout	Yes
4a	FC-(N1), Sigmoid	Yes
4b	FC-(N10), Softmax	Yes

Table 7: Unsupervised Domain Adaptation Results

Method	MNIST→USPS	USPS→MNIST
No adap.	74.14	78.69
CoGAN	95.65	93.15
UNIT (proposed)	95.97	93.58

put layer has 10 output neurons representing the digit class (4b in Table 6). We used the labeled training samples from the source domain to train the classifier and used the unlabeled samples in the target domain as well as the samples in the source domain to learn the image translation function. For adapting a classifier from the MNIST domain to the USPS domain, the training data included the labeled

Table 8: The adversarial discriminator architecture for the SVHN-MNIST domain adaptation problem.

Layer	Discriminators	Shared?
1	CONV-(N64,K5,S1), MaxPooling-(K2,S2)	No
2	CONV-(N128,K5,S1), MaxPooling-(K2,S2)	Yes
3	CONV-(N256,K5,S1), MaxPooling-(K2,S2)	Yes
4	CONV-(N512,K5,S1), MaxPooling-(K2,S2)	Yes
5a	FC-(N1), Sigmoid	Yes
5b	FC-(N10), Softmax	Yes

Table 9: Unsupervised Domain Adaptation Results

Method	Accuracy
SA (Fernando et al., 2013)	59.32%
DANN (Ganin et al., 2016)	73.85%
DTN (Taigman et al., 2017)	84.88%
UNIT (proposed)	90.53%

MNIST training set and the unlabeled USPS training set. We reported the performance of the adapted classifier in classifying the USPS test set. For adapting a classifier from the USPS domain to the MNIST domain, the training data included the labeled USPS training set and the unlabeled MNIST training set. We reported the performance of the adapted classifier in classifying the MNIST test set. We compared the performance of the proposed method with the CoGAN algorithm (Liu & Tuzel, 2016), which was the state-of-the-art approach for this domain adaptation task. The results are reported in Table 7. From the table, we found that UNIT’s performance was comparable to CoGAN.

In the second UDA experiment, we applied the above approach to the task of adapting a classifier from the Street View House Number (SVHN) dataset (Netzer et al., 2011) to the MNIST dataset. Specifically, we trained the UNIT network to learn to translate images between the SVHN and MNIST training sets as well as to classify the digit classes in the SVHN training images using the features extracted from the SVHN domain adversarial discriminators. In the test time, we applied the target domain adversarial discriminator to classify the digit class for the images in the MNIST test set. We used a UNIT network where the encoder and decoder architecture were the same as those shown in Table 3. But the adversarial discriminators were based on a network architecture similar to the one used in as shown in (Taigman et al., 2017). The details of the discriminator architecture is given in Table 8. The adversarial discriminators had two different output layers: the first output layer has a single output neuron representing the probability that an input sample was from the training dataset (5a in Table 8) and the other output layer has 10 output neurons representing the digit class (5b in Table 8). We reported the

achieved performance with comparison to the competing methods in Table 9. We found that our approach achieved a 90.53% accuracy, which was much better than 84.88% achieved by the previous state-of-the-art method (Taigman et al., 2017).

D. Network Architecture

The UNIT architecture for translating natural images presented in the experiment section is shown in Table 10.

E. Additional Translation Results

Additional unsupervised image-to-image translation results are visualized in Figure 14, 15, 16, 17 18, and 19.

Unsupervised Image-to-Image Translation Networks

Table 10: The UNIT network architecture for translating natural images in the experiment section. N=Neurons, K=Kernel size, S=Stride size, BN=Batch Normalization

Encoder Layer	Input	Encoders	Weight-sharing?
1	Images	CONV-(N64,K5,S2), BN, LeakyReLU	No
2	Output from Encoder Layer 1	CONV-(N128,K5,S2), BN, LeakyReLU	No
3	Output from Encoder Layer 2	CONV-(N256,K5,S2), BN, LeakyReLU	Yes
4	Output from Encoder Layer 3	CONV-(N512,K5,S2), BN, LeakyReLU	Yes
5	Output from Encoder Layer 4	CONV-(N1024,K5,S2), BN, LeakyReLU	Yes
Latent Space	Input	Letent space	Shared?
μ_1	Output from Encoder Layer 2	CONV-(N256,K1,S1)	Yes
σ_1^2	Output from Encoder Layer 2	CONV-(N256,K1,S1), Soft-plus	Yes
μ_2	Output from Encoder Layer 3	CONV-(N512,K1,S1)	Yes
σ_2^2	Output from Encoder Layer 3	CONV-(N512,K1,S1), Soft-plus	Yes
μ_3	Output from Encoder Layer 4	CONV-(N1024,K1,S1)	Yes
σ_3^2	Output from Encoder Layer 4	CONV-(N1024,K1,S1), Soft-plus	Yes
μ_4	Output from Encoder Layer 5	CONV-(N2048,K1,S1)	Yes
σ_4^2	Output from Encoder Layer 5	CONV-(N2048,K1,S1), Soft-plus	Yes
Generator Layer	Input	Generators	Weight-sharing?
1	$z_4 \sim \mathcal{N}(\mu_4, \sigma_4^2 I)$	DCONV-(N1024,K6,S2), BN, LeakyReLU	Yes
2	$z_3 \sim \mathcal{N}(\mu_3, \sigma_3^2 I) +$ Output from Generator Layer 1	DCONV-(N512,K5,S2),BN,LeakyReLU	Yes
3	$z_2 \sim \mathcal{N}(\mu_2, \sigma_2^2 I) +$ Output from Generator Layer 2	DCONV-(N256,K5,S2),BN,LeakyReLU	Yes
4	$z_1 \sim \mathcal{N}(\mu_1, \sigma_1^2 I) +$ Output from Generator Layer 2	DCONV-(N128,K6,S2),BN,LeakyReLU	Yes
5	Output from Generator Layer 4	DCONV-(N64,K6,S2), BN, LeakyReLU	No
6	Output from Generator Layer 5	DCONV-(N3 or N1), TanH	No
Discriminator Layer	Input	Discriminators	Weight-sharing?
1	Images or Output from Generator Layer 6	CONV-(N64,K5,S2), BN, LeakyReLU	No
2	Output from Discriminator Layer 1	CONV-(N128,K5,S2), BN, LeakyReLU	No
3	Output from Discriminator Layer 2	CONV-(N256,K5,S2), BN, LeakyReLU	Yes
4	Output from Discriminator Layer 3	CONV-(N512,K5,S2), BN, LeakyReLU	Yes
5	Output from Discriminator Layer 4	CONV-(N1024,K5,S2), BN, LeakyReLU	Yes
6	Output from Discriminator Layer 5	CONV-(N2048,K5,S2), Sigmoid	Yes

Unsupervised Image-to-Image Translation Networks

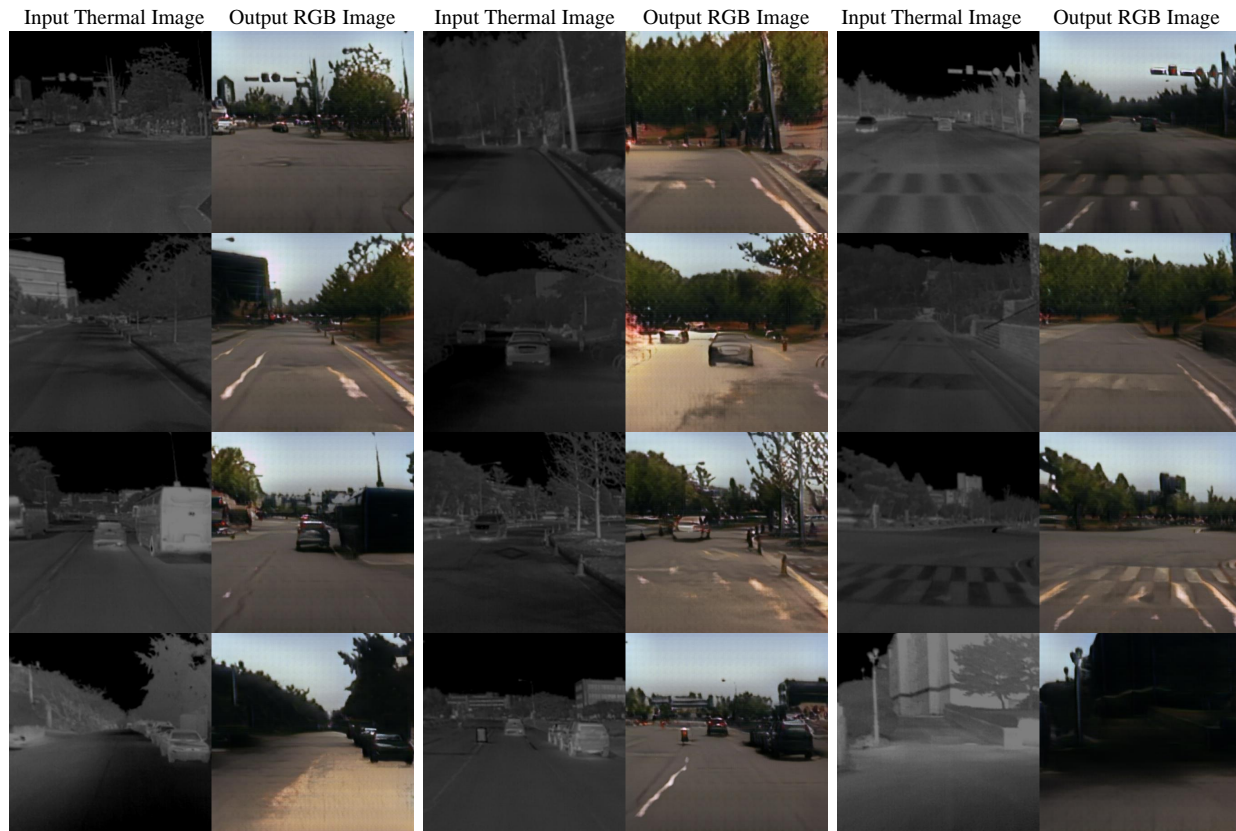


Figure 14: Thermal IR to Color Image Translation



Figure 15: Color to Thermal IR Image Translation

Unsupervised Image-to-Image Translation Networks



Figure 16: Day-time to Night-time Image Translation

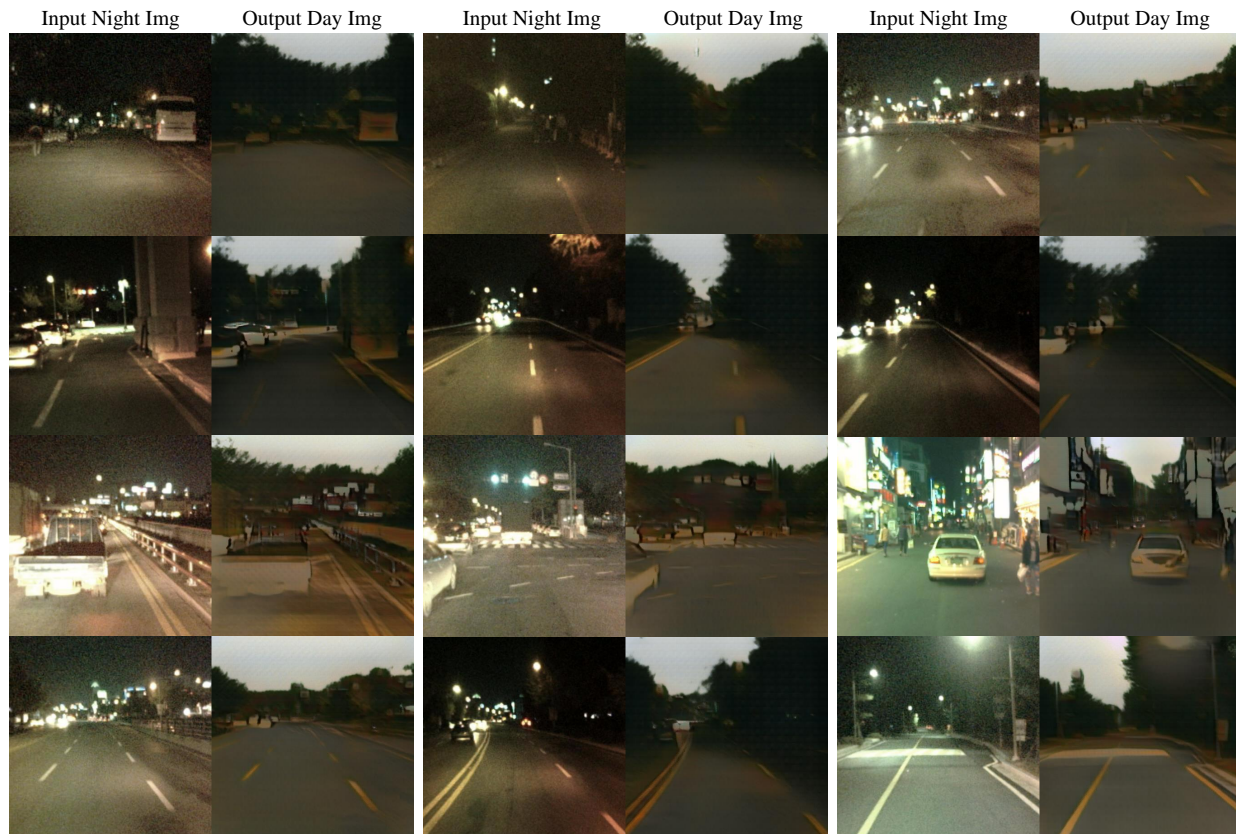


Figure 17: Night-time to Day-time Image Translation

Unsupervised Image-to-Image Translation Networks



Figure 18: Sunny to Rainy Image Translation



Figure 19: Rainy to Sunny Image Translation